

Formation of $C_{\text{NHC}}^{\wedge}C_{\text{alkyl}}$ and $C_{\text{NHC}}^{\wedge}C_{\text{aryl}}$ κ^2 -Chelate Complexes through Competitive sp^3 - and sp^2 -CH Activations: An Experimental and Computational Study

Matthias D. Böhme, Sebastian Termühlen, Patrick D. Dutschke, Alexander Hepp, and F. Ekkehardt Hahn*



Cite This: *ACS Omega* 2023, 8, 48515–48521



Read Online

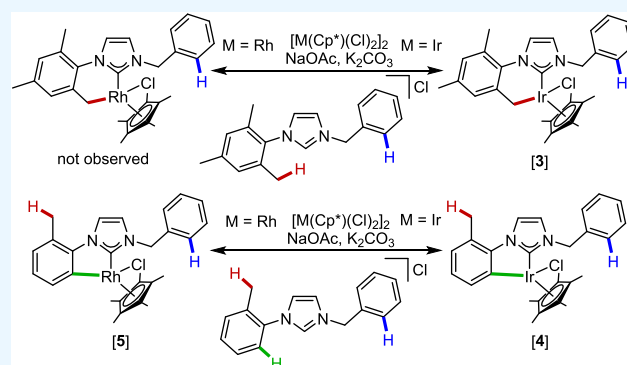
ACCESS |

Metrics & More

Article Recommendations

Supporting Information

ABSTRACT: Depending on the chelate ring present, cyclometalated complexes are useful catalysts for various reactions. The reactivity of Ir^{III} and Rh^{III} NHC complexes bearing aliphatic or aromatic N,N' -substituents and thus featuring various metalation sites toward cyclometalation has been investigated. The Rh^{III} complex bearing an N -methyl- N' -benzyl-NHC does not participate in any cyclometalation, while the Ir^{III} complex reacts under metalation of an *ortho*-methyl group of the Mes substituent to give complex [3] with a six-membered chelate ring. The Rh^{III} and Ir^{III} complexes bearing an N -*o*-tolyl- N -benzyl-NHC undergo sp^2 -CH activation to yield the cyclometalated complexes [4] and [5] featuring a five-membered $C_{\text{NHC}}^{\wedge}C$ chelate ring. Density functional theory (DFT) studies corroborated the experimental findings.



INTRODUCTION

In the past few decades, various N -heterocyclic carbenes (NHCs) have been shown to be valuable ligands for the preparation of organometallic complexes. The interest in NHCs as ligands is based on their broad range of stereo-electronic properties¹ and consequently the use of their complexes as efficient catalysts² for various transformations.

Intramolecular CH activation at the N -substituents of NHCs has been utilized to create unique $C_{\text{NHC}}^{\wedge}C$ chelate complexes. A variety of sp^3 - and sp^2 -CH activations have been described. While the sp^2 -CH activation has been mainly used to create five-membered chelate rings from N -aryl³ or six-membered chelate rings from N -alkyl(aryl) NHCs,⁴ the sp^3 -CH activation has been observed for NHCs featuring N -alkyl substituents (Scheme 1, top).^{5ab} Orthometalation involving a phenylphosphine donor has also been observed in titanium alkylidene complexes.^{5c}

In 2009, Sola et al. demonstrated the possibility to activate a methyl group of the mesityl substituents on an N,N' -dimethyl-NHC iridium complex, albeit through an elaborate protocol (Scheme 1, bottom). The reversibility of the chelate complex formation was also demonstrated.⁶

In this study, we compare the reactivity of Ir^{III} and Rh^{III} NHC complexes featuring different N,N' -substituents at the NHCs toward the activation of sp^2 - and sp^3 -CH bonds at these substituents to yield five- or six-membered chelate rings by a base-mediated reaction. Specifically, two imidazolium salts, 1(Cl) and 2(Cl) (Figure 1) featuring various possible sp^2 - and

sp^3 -CH sites for cyclometalation reactions, were prepared and reacted with Rh^{III} and Ir^{III} complexes.

Ligand precursor 1(Cl) contains two different potential sites, C10–H and C14–H, for a cyclometalation reaction. In both cases, a six-membered chelate ring would be formed from either an sp^2 -CH activation (Figure 1, blue) or an sp^3 -CH activation (Figure 1, red). For ligand precursor 2(Cl), an additional reaction is possible. Here, a five-membered chelate ring could form by sp^2 -CH activation at the *ortho*-position of the *o*-tolyl substituent (Figure 1, green).

RESULTS AND DISCUSSION

In the first experiment, the reactivity of the C14–H and C10–H bonds in the NHC complex obtained from 1(Cl) was studied (Scheme 2). Imidazolium salt 1(Cl) (2.0 equiv) was reacted with $[\text{Ir}(\text{Cp}^*)(\text{Cl})_2]_2$ (1.0 equiv) or $[\text{Rh}(\text{Cp}^*)(\text{Cl})_2]_2$ (1.0 equiv) in the presence of K_2CO_3 (4.0 equiv) and NaOAc (8.0 equiv) under conditions known to give cyclometalated $C_{\text{NHC}}^{\wedge}C$ complexes. In case cyclometalation occurs, it would lead to a six-membered $C_{\text{NHC}}^{\wedge}C$ chelate ring involving either

Received: October 25, 2023

Accepted: November 10, 2023

Published: December 5, 2023



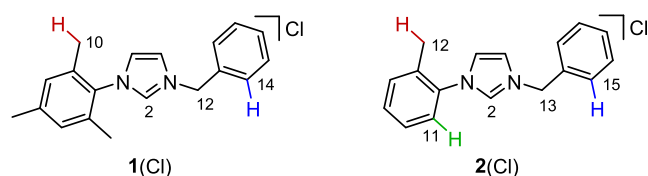
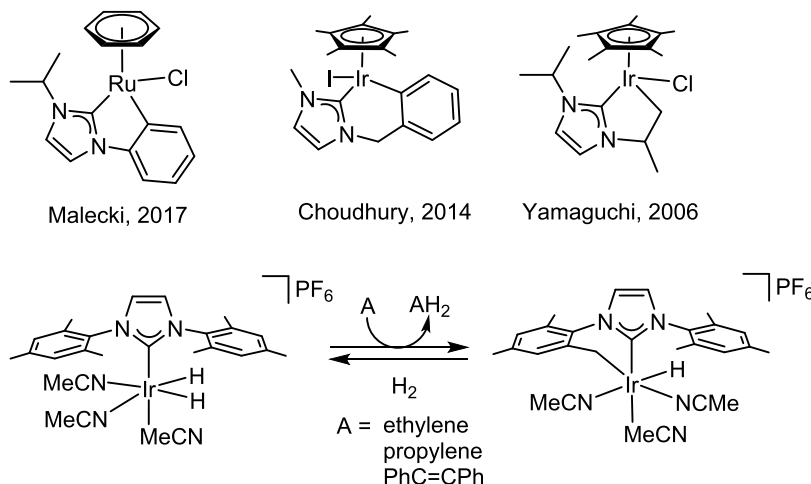
Scheme 1. C_{NHC}[^]C Chelate Complexes (Top) and Reversible sp³-CH Activation at an Iridium Complex (Bottom)

Figure 1. Ligand precursors 1(Cl) and 2(Cl) were used for competitive cyclometalation studies.

sp³ carbon atom C10^{6a} or sp² carbon atom C14 (Scheme 2).⁴ Thus, the ring size may not be essential to determine which CH bond in the intermediate NHC complex is activated.

From the reactions depicted in Scheme 2, only the iridium complex [3] could be isolated. The reaction of 1(Cl) with [Ir(Cp*)(Cl)₂]₂ yields exclusively the C_{NHC}[^]C chelate complex based on activation of an sp³-CH bond of the mesitylene substituent. No characterized reaction products could be isolated from the reaction of 1(Cl) with [Rh(Cp*)(Cl)₂]₂. The reaction mixture turned black, and an insoluble black precipitate formed within 1 h (Scheme 2).

The isolated Ir^{III} NHC complex [3] was fully characterized by NMR spectroscopy, HR mass spectrometry, and elemental

analysis (see the SI) and an X-ray diffraction study (Figure 2). The ¹H NMR spectrum of [3] does not feature the resonance

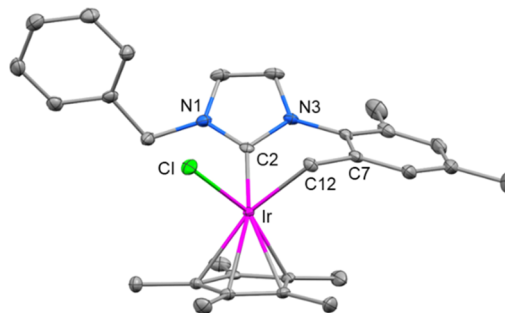
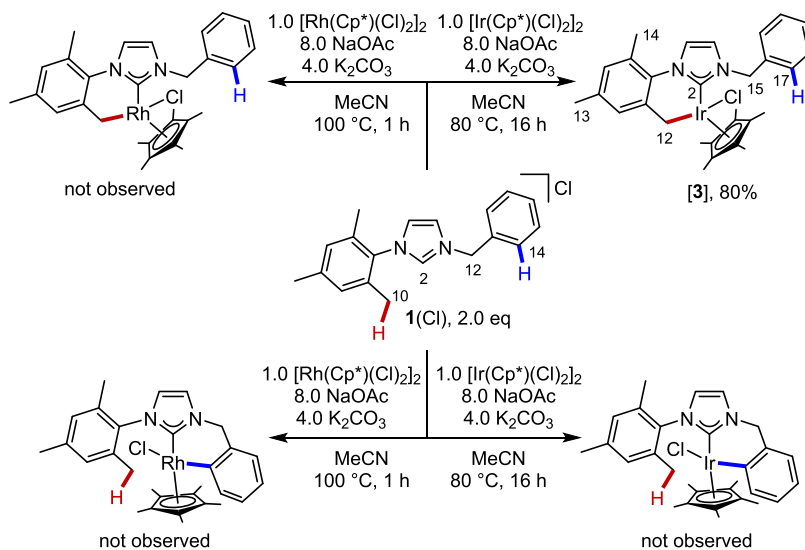
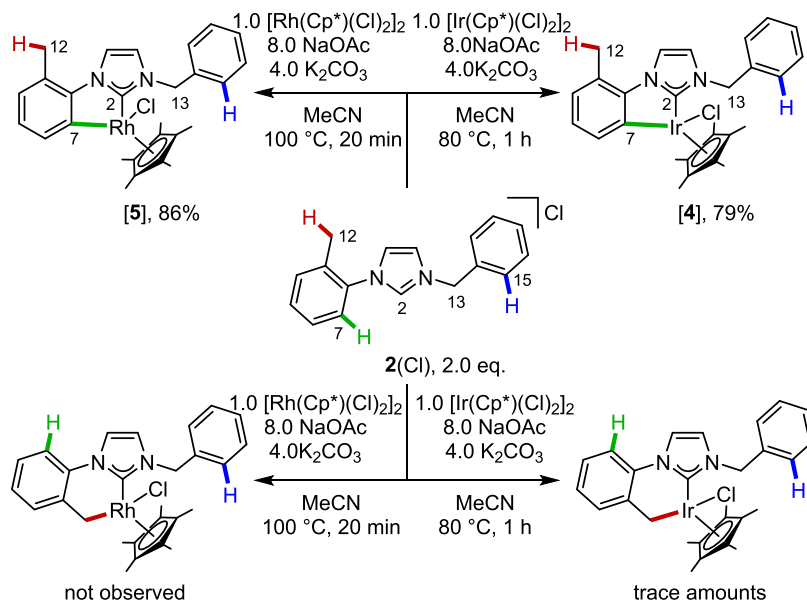


Figure 2. Molecular structure of complex [3] (hydrogen atoms have been omitted for clarity and 50% probability ellipsoids are depicted). Selected bond lengths (Å) and angles (deg): Ir–Cl 2.4178(5), Ir–C2 1.993(2), Ir–C12 2.119(2); range Ir–C_{Cp*} 2.141(2)–2.246(2), N1–C2 1.351(3), N3–C2 1.378(3); Cl–Ir–C2 90.19(6), Cl–Ir–C12 85.16(5), C2–Ir–C12 79.70(8), Ir–C2–N1 129.37(15), Ir–C2–N3 125.96(14), N1–C2–N3 104.57(16), Ir–C12–C7 110.72(13).

Scheme 2. Possible Reaction Products of the Competitive Cyclometalation of [Ir(Cp*)(Cl)₂]₂ or [Rh(Cp*)(Cl)₂]₂ with 1(Cl)

Scheme 3. Possible Reaction Products of the Competitive Cyclometalation of $[\text{Ir}(\text{Cp}^*)(\text{Cl})_2]_2$ or $[\text{Rh}(\text{Cp}^*)(\text{Cl})_2]_2$ with $2(\text{Cl})$ 

for the imidazolium H2 proton anymore, which was observed at $\delta = 11.12$ ppm for **1(Cl)**,⁷ indicating the formation of an $\text{Ir}^{\text{III}}\text{-NHC}$ complex. The resonance for the protons of the bridging methylene group (C12–H) was observed as a singlet at $\delta = 5.86$ ppm for **1(Cl)** and was recorded for **[3]** as two doublets at $\delta = 5.79$ (H15) and 5.63 (H15') ppm with a coupling constant of $^2J_{\text{HH}} = 15.3$ Hz indicative for diastereomeric protons caused by the stereocenter at the metal atom. Significant changes were observed for the resonances of the mesitylene methyl groups upon the cyclometalation of **1(Cl)**. For **1(Cl)**, two resonances for the methyl protons were recorded at $\delta = 2.32$ ppm (3H, *para*- CH_3) and $\delta = 2.03$ ppm (6H, *ortho*- CH_3). For **[3]**, a singlet at $\delta = 2.29$ ppm (3 H) can be assigned to the H14 protons. The resonance for methyl protons H13 was recorded at $\delta = 2.30$ ppm. The H12 protons were observed as two doublets at $\delta = 3.73$ ppm (H12) and $\delta = 2.39$ ppm (H12') with a coupling constant of $^2J_{\text{HH}} = 10.5$ Hz. This clearly demonstrated the formation of an unsymmetrical mesityl group and metalation of carbon atom C12.

The $^{13}\text{C}\{^1\text{H}\}$ NMR spectrum corroborated the formation of an unsymmetric mesityl group in **[3]** by displaying six resonances for the aromatic mesityl carbon atoms. Three resonances were observed for carbon atoms C12–C14. Two of these at $\delta = 20.9$ ppm (C13) and $\delta = 19.9$ ppm (C14) fall in the range typical for mesityl CH_3 groups. The resonance for C12 was observed significantly upfield at $\delta = 8.2$ ppm. Based on the high-field shift of the resonance for C12 compared to those of C13 and C14, the metalation of C12 can be concluded. The expected four resonances in the typical range were observed for the aromatic carbon atoms of the benzyl group, confirming that this group did not participate in the cyclometalation. The resonance for the carbene carbon atom C2 was observed at $\delta = 168.9$ ppm and falls in the typical range for cyclometalated Ir^{III} NHC complexes.^{3b–d,4}

The HR mass spectrum (ESI, positive ions) supports the formation of the cyclometalated Ir^{III} NHC complex³ with the strongest peak observed at $m/z = 603.2343$ (calcd. for $[[\text{3}]\text{-Cl}]^+$ 603.2352). However, this observation does not support the cyclometalation involving the mesitylene group as

cyclometalation involving the benzyl group would lead to the same mass.

The molecular structure of **[3]** was unequivocally established by a single-crystal X-ray diffraction study (Figure 2), confirming the formation of a six-membered chelate ring by $\text{sp}^3\text{-CH}$ activation of one methyl group of the ligand precursor **1(Cl)**. The iridium atom is coordinated in the piano-stool geometry. The six-membered metalacycle adopts the half-chair conformation, with the $\text{Ir}\text{-C12}$ bond length of 2.119(2) Å being significantly longer than the $\text{Ir}\text{-C2}$ separation of 1.993(2) Å. The metalacycle appears to be unstrained with a $\text{C2}\text{-Ir}\text{-C12}$ bite angle of 79.70(8)° and an $\text{Ir}\text{-C12}\text{-C7}$ angle of 110.72(13)°.

For the synthesis of **[3]**, two bases, K_2CO_3 and NaOAc, were used. Most likely, the bases first deprotonated the C2 position of the imidazolium cation, allowing the formation of the Ir^{III} NHC complex.

The sodium acetate can then also act as a ligand, substituting the chlorido ligands to give an acetato complex. This complex then undergoes a rearrangement under elimination of acetic acid and formation of the final $\text{C}_{\text{NHC}}^{\wedge}\text{C}$ chelate complex.⁸ At this point, we were surprised to find experimentally that the orthometalation involves a mesitylene CH_3 group ($\text{sp}^3\text{-CH}$ activation) instead of the *ortho*- $\text{C}\text{-H}$ bond of the *N*-benzyl substituent ($\text{sp}^2\text{-CH}$ activation). We assume that the steric situation is responsible for the preferred $\text{sp}^3\text{-CH}$ activation relative to the $\text{sp}^2\text{-CH}$ activation. Regardless of the rotation about the $\text{N}\text{-C}_{\text{mesityl}}$ bond, one *o*-methyl group always points more or less toward the metal center, while the aromatic benzyl $\text{C}\text{-H}$ groups can completely rotate away from the metal center.

In the second experiment, ligand precursor **2(Cl)** was used. In addition to the cyclometalation sites present in **1(Cl)**, compound **2(Cl)** features an additional metalation site at carbon atom C11 (Figure 1, right), allowing the formation of a five-membered $\text{C}_{\text{NHC}}^{\wedge}\text{C}$ metalacycle through $\text{sp}^2\text{-CH}$ activation. We concluded from the previous experiment that $\text{sp}^3\text{-CH}$ activation can be preferred over $\text{sp}^2\text{-CH}$ activation if the cyclometalation results in a six-membered ring. We were intrigued to learn if the formation of a five-membered

metalacycle possible with $2(\text{Cl})$ would be preferred over the formation of a six-membered $\text{C}_{\text{NHC}}^{\wedge}\text{C}$ chelate ring.

Imidazolium salt $2(\text{Cl})$ was reacted with $[\text{Ir}(\text{Cp}^*)(\text{Cl})_2]_2$ or $[\text{Rh}(\text{Cp}^*)(\text{Cl})_2]_2$ under conditions similar to those employed for the preparation of [3] (Scheme 3). The reaction with $[\text{Rh}(\text{Cp}^*)(\text{Cl})_2]_2$ yielded after a short reaction time of only 20 min exclusively the chelate complex [5] through $\text{sp}^2\text{-CH}$ activation at carbon atom C7. In the reaction of $2(\text{Cl})$ with $[\text{Ir}(\text{Cp}^*)(\text{Cl})_2]_2$, the isostructural complex [4] was obtained together with a trace amount (<5% in NMR spectra of the crude reaction product) of the complex formed by $\text{sp}^3\text{-CH}$ activation at the *o*-tolyl methyl group. The main reaction products of both reactions [4] and [5] were fully characterized by NMR spectroscopy, HR mass spectrometry, elemental analysis (see the Si), and single-crystal X-ray diffraction studies (Figure 3).

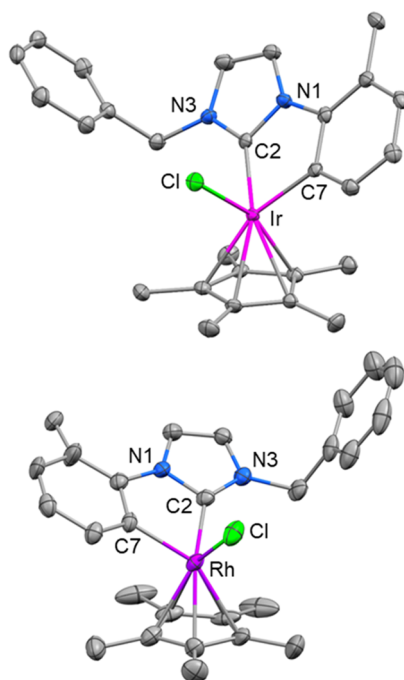


Figure 3. Molecular structures of complexes [4] (top) and [5] (bottom). Hydrogen atoms have been omitted for clarity, and 50% probability ellipsoids are depicted. Selected bond lengths (Å) and angles (deg) for [4] and [molecule A of [5]]: M–Cl 2.4006(8) [2.3994(11)], M–C2 1.975(4) [1.990(4)], M–C7 2.033(3) [2.025(4)]; range M–Cp* 2.131(3)–2.249(4) [2.119(4)–2.276(4)], N1–C2 1.362(4) [1.373(5)], N3–C2 1.350(4) [1.349(5)]; Cl–M–C2 89.14(10) [97.87(11)], Cl–M–C7 88.52(9) [91.49(12)], C2–M–C7 76.80(14) [77.73(16)], M–C2–N1 119.5(2) [115.9(3)], M–C2–N3 135.6(3) [138.0(3)], N1–C2–N3 105.0(3) [105.0(3)].

The NMR spectra of [4] and [5] are rather similar except for the coupling between the rhodium atom and selected carbon atoms. In the ^1H NMR spectra, the protons of the bridging methylene group H13 give two doublet resonances at $\delta = 5.78$ and 5.29 ppm for [4] ($\delta = 5.81$ and 5.31 ppm for [5]) with a coupling constant of $^2J_{\text{HH}} = 14.3$ Hz for [4] ($^2J_{\text{HH}} = 14.0$ Hz for [5]). As was observed for [3], the methylene protons H13 are diastereotopic and are caused by the stereocenter at the metal atom. Contrary to complex [3], the NMR spectra of complexes [4] and [5] each feature only one singlet resonance for methyl protons H12 at $\delta = 2.56$ ppm for [4] and $\delta = 2.52$

ppm for [5]. The resonance for the aryl proton H7 of ligand precursor $2(\text{Cl})$ was no longer observed in [4] or [5]. These observations indicate that the cyclometalation proceeded with the formation of a five-membered chelate ring. The HR mass spectra for both complexes support the formation of a cyclometalated complex although no information about the actual site of metalation can be drawn from the MS spectra.

In the $^{13}\text{C}\{^1\text{H}\}$ NMR spectrum of complex [4], the resonance for the carbene carbon atom C2 was observed at $\delta = 167.5$ ppm. The resonance at $\delta = 143.0$ ppm was assigned to carbon atom C7 by 2D NMR spectroscopy. The low-field resonance for C7 suggests coordination with the metal center. The $^{13}\text{C}\{^1\text{H}\}$ NMR spectrum of complex [5] is more informative due to Rh–C couplings. Both the resonances of C2 ($\delta = 185.3$ ppm) and C7 ($\delta = 159.3$ ppm) were recorded as doublets with coupling constants of $^1J_{\text{RhC}} = 55.6$ Hz and $^1J_{\text{RhC}} = 33.5$ Hz, respectively.

The coordination geometry and connectivity in [4] and [5] were established by single-crystal X-ray diffraction analyses. These analyses confirmed the formation of five-membered $\text{C}_{\text{NHC}}^{\wedge}\text{C}$ chelate complexes through $\text{sp}^2\text{-CH}$ activation at carbon atom C7 (Figure 3; for [5], only metric parameters of one of the two independent formula units in the asymmetric unit are listed). The metal centers in [4] and [5] are hexacoordinated, and the complexes adopt the piano-stool geometry. While the six-membered $\kappa^2\text{-C}_{\text{NHC}}^{\wedge}\text{C}$ ligand in [3] was observed in the half-chair conformation, the chelate ligand in [4] and [5] is nearly planar. The metric parameters in [4] and [5] are closely related. The M–C2 and M–C7 bond distances are identical within experimental error in both complexes with the M–C2 separations shorter than the M–C7 distances. The C2–M–C7 bite angles of the five-membered chelate ligands in [4] and [5] fall in the range observed for the C2–Ir–C12 bite angle of the six-membered chelate ligand in [3].

The minor side product observed in the synthesis of iridium complex [4] led to resonances in the ^1H NMR spectrum, which are very similar to those of complex [3]. We therefore assumed that the side product results from metalation of carbon atom C12 via $\text{sp}^3\text{-CH}$ activation. Indications for this $\text{sp}^3\text{-CH}$ activation are also provided by the observation of two doublets for the protons H12 indicative of metalation of the former methyl group of the ligand precursor $2(\text{Cl})$ and formation of a six-membered $\text{C}_{\text{NHC}}\text{-Ir-C}$ chelate ring. The minute amount of the side product isolated prevented its further characterization. The amount of the side product of [4] could not be increased by lengthening of the reaction time or by increasing the reaction temperature, both changes leading to the decomposition of [4].

In order to confirm some of the experimental results, density functional theory (DFT) calculations on the metalation of $2(\text{Cl})$ with rhodium were performed. Related calculations on the orthometalation of rhodium complexes bearing phenyl-substituted pyrrol^{8a} or NHC^{8b,c} ligands have been described. These calculations employed an acetato complex as an active species for the cyclometalation by $\text{sp}^2\text{-CH}$ activation at the phenyl substituent. Given the reaction conditions used for the cyclometalation of $2(\text{Cl})$, the formation of an acetato complex in situ is also very likely. Thus, rhodium NHC complexes with an acetato ligand instead of complexes with chlorido ligands were used as starting points for the calculations. Calculations for both iridium complex [4] and rhodium complex [5] were performed. In addition, the benzyl group in $2(\text{Cl})$ was

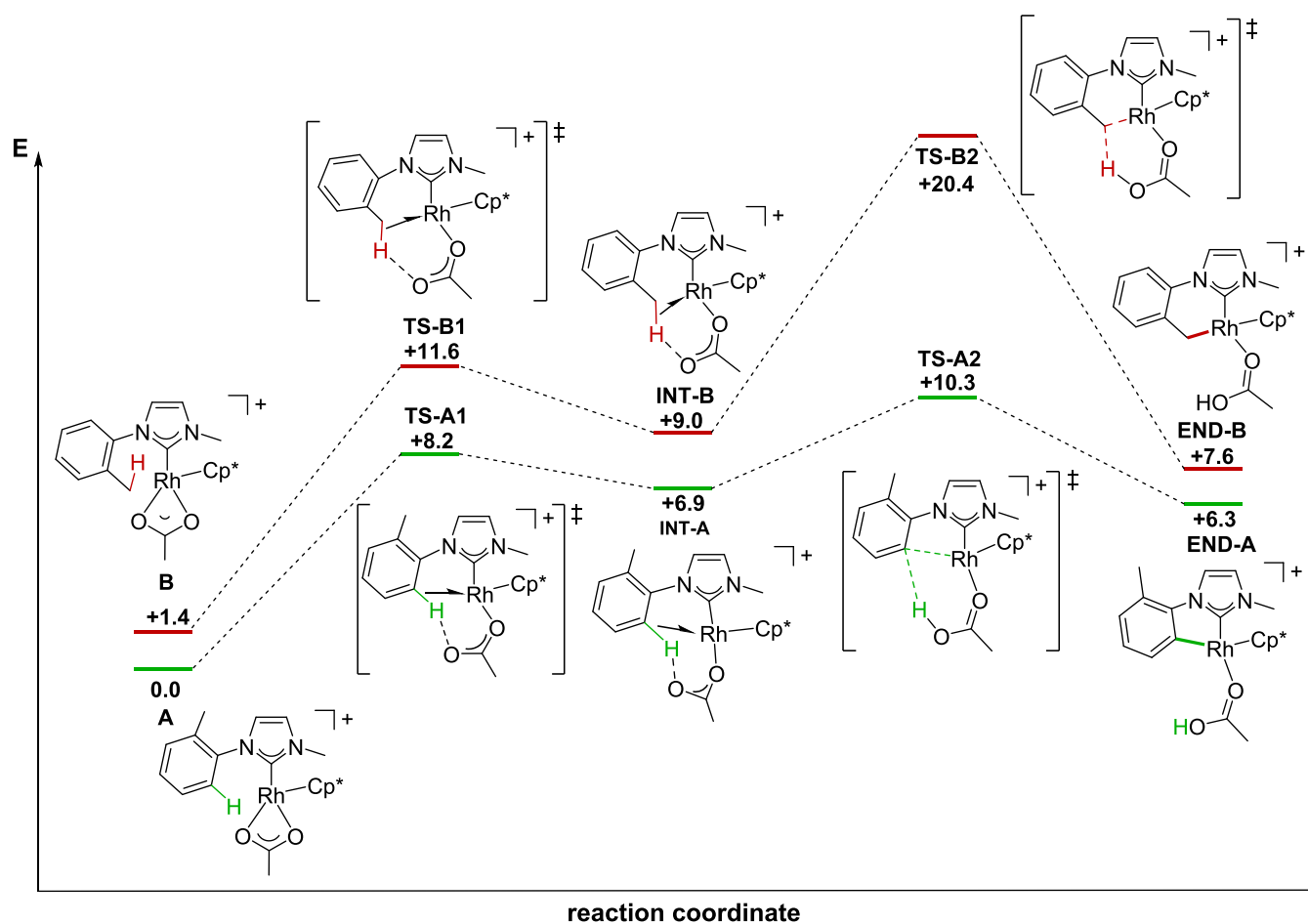


Figure 4. Calculated reaction pathways for the sp^2 - and sp^3 -CH activations with an Rh NHC acetato complex to give complex [5]. All free energies (kcal·mol⁻¹) are relative to A.

substituted for a methyl group since the benzyl group did not participate in any cyclometalation reaction studied here. This substitution reduced the number of atoms and the degrees of freedom of the molecule and thus reduced the time needed for calculations significantly. Calculations were carried out for the sp^2 -CH activation with the formation of a five-membered chelate ligand and for the sp^3 -CH activation with the formation of a six-membered chelate from ligand precursor 2(Cl). The free-energy profiles for both possible pathways for rhodium complex [5] are depicted in Figure 4, and those for iridium complex [4] are shown in the SI.

All geometries were optimized using the BP86 functional⁹ and def2-svp as the basis set.⁹ For the final calculations of all free energies, the def2-TZVPP¹⁰ basis set was used. Solvent (CPCM approach¹¹) and dispersion effect (Grimme's parameter set¹²) corrections have been applied. All structures were calculated as positively charged species with the counterions omitted (see the computational details section in the SI for additional information regarding the computational studies).

For rhodium complex [5], the starting point B for the sp^3 -CH activation is by 1.4 kcal·mol⁻¹ higher in energy than structure A caused by different orientations of the *o*-methyl group relative to the metal center. The first transition state in both pathways (TS-A1 or TS-B1) is characterized by the detachment of one oxygen of the acetato ligand from the metal center and the simultaneous formation of an agostic

interaction. Transition state TS-A1 is energetically favored ($\Delta G = +8.2$ kcal·mol⁻¹) relative to transition state TS-B1 ($\Delta G = +11.6$ kcal·mol⁻¹). In pathway B, it is not the proton closest to the acetato ligand but the proton closest to the metal center that participates in the reaction. For an optimal interaction, the methyl group must rotate in the appropriate position. Both intermediates (INT-B and INT-A) feature an O···H–C hydrogen bond.⁸ Both intermediates are rather similar in energy, with $\Delta G = 6.9$ kcal·mol⁻¹ for INT-A and $\Delta G = 9.0$ kcal·mol⁻¹ for INT-B.

The second transition state involves breaking of the C–H bond concurrently with the movement of the liberated proton closer to the oxygen atom of the acetato ligand and the coordination of the carbon atom to Rh. Pathway A ($\Delta G = +10.3$ kcal·mol⁻¹) of the sp^2 -CH activation is energetically highly favored compared to pathway B ($\Delta G = +20.4$ kcal·mol⁻¹). Finally, the acetato ligand is protonated, and the Rh–C bond is formed. This completes the cyclization reaction.

The product END-A ($\Delta G = +6.3$ kcal·mol⁻¹) with the five-membered chelate ring is energetically slightly favored over the product END-B ($\Delta G = +7.6$ kcal·mol⁻¹) with the six-membered chelate ring. The last, not calculated, step to yield the final reaction product is a ligand substitution of the acetic acid for a chlorido ligand. The calculations support the experimental findings regarding the preferred sp^2 -CH activation under the formation of the five-membered chelate

ring. Similar results were obtained for the reaction of iridium complex [4] (see the SI).

While the energy barrier for pathway A (TS-A2 $\Delta G = +10.3$ kcal·mol⁻¹) is rather low, heating to 100 °C for 20 min was required since the reactants are poorly soluble in acetonitrile. The reaction proceeds also at lower temperature, albeit much slower.

Attempts to calculate the free-energy profiles for the reaction of 1(Cl) with rhodium or iridium proved difficult due to the possible rotation of the mesityl and benzyl groups preventing a facile geometry optimization and requiring excessive computational time. The experimental data, however, clearly demonstrated the sp³-CH activation with pro-ligand 1(Cl).

CONCLUSIONS

In an experimental study, we compared the reactivity of Ir^{III} and Rh^{III} NHC complexes to undergo cyclometalation by either sp²- or sp³-CH activation at the NHC substituents. In the first scenario, where both sp²- and sp³-CH activations leading to six-membered C_{NHC}^C chelate complexes were possible, the sp³-CH activation is favored and no sp²-CH activation was observed. However, this was observed only for Ir^{III} complexes, while no cyclometalated complexes were obtained with Rh^{III}. In a second study, sp²- and sp³-CH activations were compared where the sp²-CH activation would lead to a five-membered metalacycle, while the sp³-CH activation would result in a six-membered chelate ring. In this situation, the sp²-CH activation was clearly preferred, with both Rh^{III} and Ir^{III}. Preliminary DFT calculations corroborated the experimental findings regarding the preferred formation of a five-membered chelate ring by sp²-CH activation.

ASSOCIATED CONTENT

Supporting Information

The Supporting Information is available free of charge at <https://pubs.acs.org/doi/10.1021/acsomega.3c08427>.

Summary of ¹H and ¹³C{¹H} NMR spectra (PDF)

xyz-tables-complex-[4] (TXT)

xyz-tables-complex-[5] (TXT)

Accession Codes

CCDC 2245902–2245904 contain the supplementary crystallographic data for this paper. These data can be obtained free of charge via www.ccdc.cam.ac.uk/data_request/cif, or by emailing data_request@ccdc.cam.ac.uk, or by contacting The Cambridge Crystallographic Data Centre, 12 Union Road, Cambridge CB2 1EZ, UK; fax: + 44 1223 336033.

AUTHOR INFORMATION

Corresponding Author

F. Ekkehardt Hahn – Institut für Anorganische und Analytische Chemie, Westfälische Wilhelms-Universität Münster, 48149 Münster, Germany; orcid.org/0000-0002-2807-7232; Email: fehahn@uni-muenster.de

Authors

Matthias D. Böhme – Institut für Anorganische und Analytische Chemie, Westfälische Wilhelms-Universität Münster, 48149 Münster, Germany

Sebastian Termühlen – Institut für Anorganische und Analytische Chemie, Westfälische Wilhelms-Universität Münster, 48149 Münster, Germany

Patrick D. Dutschke – Institut für Anorganische und Analytische Chemie, Westfälische Wilhelms-Universität Münster, 48149 Münster, Germany

Alexander Hepp – Institut für Anorganische und Analytische Chemie, Westfälische Wilhelms-Universität Münster, 48149 Münster, Germany; orcid.org/0000-0003-1288-925X

Complete contact information is available at:

<https://pubs.acs.org/10.1021/acsomega.3c08427>

Notes

The authors declare no competing financial interest.

ACKNOWLEDGMENTS

The authors acknowledge financial support from the Deutsche Forschungsgemeinschaft (IRTG 2027).

REFERENCES

- (1) (a) Merschel, A.; Glodde, T.; Neumann, B.; Stammler, H.-G.; Ghadwal, R. S. Nickel-Catalyzed Intramolecular 1,2-Aryl Migration of Mesoionic Carbenes (iMICs). *Angew. Chem., Int. Ed.* **2021**, *60*, 2969–2973. (b) Huynh, H. V. Electronic Properties of N-Heterocyclic Carbenes and Their Experimental Determination. *Chem. Rev.* **2018**, *118*, 9457–9492. (c) Dröge, T.; Glorius, F. The Measure of All Rings—N-Heterocyclic Carbenes. *Angew. Chem., Int. Ed.* **2010**, *49*, 6940–6952. (d) Correia Bicho, B. A.; Guthardt, R.; Bruhn, C.; Großhennig, D.; Orth, T.; Pfeiffer, F.; Siemeling, U. *N-tert*-Alkyl-Substituted N-Heterocyclic Carbenes with a 1,1'-Ferrocenediyl Backbone. *Eur. J. Inorg. Chem.* **2022**, e202101014. (e) Hahn, F. E.; Jahnke, M. Heterocyclic Carbenes: Synthesis and Coordination Chemistry. *Angew. Chem., Int. Ed.* **2008**, *47*, 3122–3172.
- (2) (a) Flanigan, D. M.; Romanov-Michailidis, F.; White, N. A.; Rovis, T. Organocatalytic Reactions Enabled by N-Heterocyclic Carbenes. *Chem. Rev.* **2015**, *115*, 9307–9387. (b) Bera, S. S.; Szostak, M. Cobalt–N-Heterocyclic Carbene Complexes in Catalysis. *ACS Catal.* **2022**, *12*, 3111–3137. (c) Lee, J.; Hahn, H.; Kwak, J.; Kim, M. New Aspects of Recently Developed Rhodium(N-Heterocyclic Carbene)-Catalyzed Organic Transformations. *Adv. Synth. Catal.* **2019**, *361*, 1479–1499. (d) Iglesias, M.; Oro, L. A. A leap forward in iridium–NHC catalysis: new horizons and mechanistic insights. *Chem. Soc. Rev.* **2018**, *47*, 2772–2808. (e) Morales-Cerón, J. P.; Lara, P.; López-Serrano, J.; Santos, L. L.; Salazar, V.; Álvarez, E.; Suárez, A. Rhodium(I) Complexes with Ligands Based on N-Heterocyclic Carbene and Hemilabile Pyridine Donors as Highly *E* Stereoselective Alkyne Hydrosilylation Catalysts. *Organometallics* **2017**, *36*, 2460–2469.
- (3) (a) Balamurugan, G.; Ramesh, R.; Malecki, J. G. Cyclometalated Ru(II)-NHC Complexes as Effective Catalysts for Transfer Hydrogenation: Influence of Wingtip Group on Catalytic Outcome. *ChemistrySelect* **2017**, *2*, 10603–10608. (b) Böhmer, M.; Kampert, F.; Tan, T. T. Y.; Guisado-Barrios, G.; Peris, E.; Hahn, F. E. Ir^{III}/Au^I and Rh^{III}/Au^I Heterobimetallic Complexes as Catalysts for the Coupling of Nitrobenzene and Benzylic Alcohol. *Organometallics* **2018**, *37*, 4092–4099. (c) Maity, R.; Koppetz, H.; Hepp, A.; Hahn, F. E. Heterobimetallic Carbene Complexes by a Single-Step Site-Selective Metalation of a Tricarbene ligand. *J. Am. Chem. Soc.* **2013**, *135*, 4966–4969. (d) Semwal, S.; Ghorai, D.; Choudhury, J. Wingtip-Dictated Cyclometalation of N-Heterocyclic Carbene Ligand Framework and Its Implication toward Tunable Catalytic Activity. *Organometallics* **2014**, *33*, 7118–7124. (e) Borah, D.; Sah, B.; Sarma, B.; Das, P. A cyclometalated Ir(III)-NHC complex as recyclable catalyst for acceptorless dehydrogenation of alcohols to carboxylic acids. *Dalton Trans.* **2020**, *49*, 16866–16876.
- (4) (a) Semwal, S.; Mukkatt, I.; Thenarukandiyil, R.; Choudhury, J. Small “Yaw” Angles, Large “Bite” Angles and an Electron-Rich Metal: Revealing a Stereoelectronic Synergy To Enhance Hydride-Transfer Activity. *Chem. - Eur. J.* **2017**, *23*, 13051–13057. (b) Kaur, M.; Patra, K.; Din Reshi, N. U.; Bera, J. K. Base-Controlled Direct Synthesis of

Metal–Methyleneimidazoline (MIz) and Metal–Mesoionic (MIC) Compounds. *Organometallics* **2020**, *39*, 189–200.

(5) (a) Hanasaka, F.; Tanabe, Y.; Fujita, K.-i.; Yamaguchi, R. Synthesis of New Iridium N-Heterocyclic Carbene Complexes and Facile Intramolecular Alkyl C–H Bond Activation Reactions of the Carbene Ligand. *Organometallics* **2006**, *25*, 826–831. (b) Tanabe, Y.; Hanasaka, F.; Fujita, K.-i.; Yamaguchi, R. Scope and Mechanistic Studies of Intramolecular Aliphatic C–H Bond Activation of N-Heterocyclic Carbene Iridium Complexes. *Organometallics* **2007**, *26*, 4618–4626. (c) van Doorn, J. A.; van der Heijden, H.; Orpen, A. G. Tantalum and Titanium Alkylidene Complexes Bearing Phosphinoalkoxide Ligands. Reversible Ortho-Metalation of a Titanium Alkylidene. *Organometallics* **1994**, *13*, 4271–4277.

(6) (a) Torres, O.; Martín, M.; Sola, E. Labile N-Heterocyclic Carbene Complexes of Iridium. *Organometallics* **2009**, *28*, 863–870. (b) Navarro, J.; Torres, O.; Martín, M.; Sola, E. Iridium Complexes of the Doubly Cyclometalated NHC ligand IMes. *J. Am. Chem. Soc.* **2011**, *133*, 9738–9740.

(7) Bouhrara, M.; Jeanneau, E.; Veyre, L.; Copéret, C.; Thieuleux, C. Dissymmetric gold(I) N-heterocyclic carbene complexes: a key unexpected structural parameter for highly efficient catalysts in the addition of alcohols to internal alkynes. *Dalton Trans.* **2011**, *40*, 2995–2999.

(8) (a) Davies, D. L.; Ellul, C. E.; Macgregor, S. A.; McMullin, C. L.; Singh, K. Experimental and DFT Studies Explain Solvent Control of C–H Activation and Product Selectivity in the Rh(III)-Catalyzed Formation of Neutral and Cationic Heterocycles. *J. Am. Chem. Soc.* **2015**, *137*, 9659–9669. (b) Tamosiunaite, N.; Logie, L. C.; Neale, S. E.; Singh, K.; Davies, D. L.; Macgregor, S. A. Experimental and Computational Studies on the Acetate-Assisted C–H Activation of N-Aryl Imidazolium Salts at Rhodium and Iridium: A Chloride Additive Changes the Selectivity of C–H Activation. *J. Org. Chem.* **2022**, *87*, 1445–1456. (c) Alharis, R. A.; McMullin, C. L.; Davies, D. L.; Singh, K.; Macgregor, S. A. The Importance of Kinetic and Thermodynamic Control when Accessing Mechanisms of Carboxylate-Assisted C–H Activation. *J. Am. Chem. Soc.* **2019**, *141*, 8896–8906.

(9) Perdew, J. P. Density-functional approximation for the correlation energy of the inhomogeneous electron gas. *Phys. Rev. B* **1986**, *33*, 8822–8824.

(10) Weigend, F.; Ahlrichs, R. Balanced basis sets of split valence, triple zeta valence and quadruple zeta valence quality for H to Rn: Design and assessment of accuracy. *Phys. Chem. Chem. Phys.* **2005**, *7*, 3297–3305.

(11) Barone, V.; Cossi, M. J. Quantum Calculation of Molecular Energies and Energy Gradients in Solution by a Conductor Solvent Model. *J. Phys. Chem. A* **1998**, *102*, 1995–2001.

(12) (a) Grimme, S.; Antony, J.; Ehrlich, S.; Krieg, H. A consistent and accurate *ab initio* parametrization of density functional dispersion correction (DFT-D) for the 94 elements H–Pu. *J. Chem. Phys.* **2010**, *132*, No. 154104. (b) Grimme, S.; Ehrlich, S.; Goerigk, L. Effect of the Damping Function in Dispersion Corrected Density Functional Theory. *J. Comput. Chem.* **2011**, *32*, 1456–1465.